STUDY OF ELASTIC AND INELASTIC SCATTERING OF ^{16}O BY ^{28}Si

by

ROBERT R. BRUCKMAN

B. A., Hastings College, 1976

A MASTER'S THESIS

submitted in partial fulfillment of the

requirements for the degree

MASTER OF SCIENCE

Department of Physics

Kansas State University

Manhattan, Kansas 66506

1978

Approved by:

John D. Eck

Major Professor

TABLE OF CONTENTS

LIST OF TABLES

LIST OF FIGURES

I. INTRODUCTION

With the advent of the Tandem Van de Graaff Accelerator it became possible to study the nuclear interaction of heavy ions over a wide range of atomic numbers and bombarding energies. Elastic and inelastic scattering are probably the least complicated of the possible nuclear interactions and are straightforward to study experimentally. By investigating the elastic and inelastic scattering cross sections much information on the nuclear interaction of heavy ions can be obtained, and in particular, the shape of the nucleus can be determined.

Many nuclei are known to be deformed. In the region of A=28, it is assumed that the deformed nuclei are axial symmetric. The radius of the surface of these nuclei can be written as

$$R = R_0 \left[1 + \sum_{\lambda=0,2,4} \beta_\lambda Y_{\lambda o}(\theta)\right] \qquad (1)$$

in the body centered coordinate system. If the quadrupole deformation, β_2, is the only non-zero term then the nucleus is deformed from a spherical shape to a shape like a watermelon (a prolate spheroid) or to a shape like a pumpkin (an oblate spheroid) depending on the sign of β_2. These deformations are shown in Figure 1. The magnitude and sign of β_2 affects how a nucleus is deformed, but it does not affect the total volume of the nucleus. Figure 2 shows how the magnitude and sign of β_2, as determined by experimental means[1], changes in the region of A=28.

For the case of a nucleus which has spherical symmetry (β_2=0), according to quantum mechanics, it would take an infinite energy to cause it to rotate as a rigid rotor. However, for a deformed nucleus ($\beta_2 \neq 0$),

EXPLANATION OF FIGURE 1

The quadrupole deformations of a nucleus.

QUADRUPOLE DEFORMATIONS

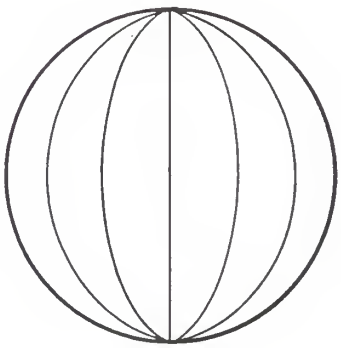

$\beta_2=0$

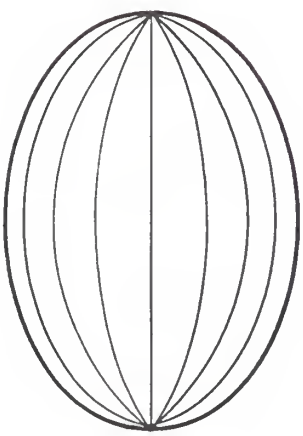

$\beta_2>0$

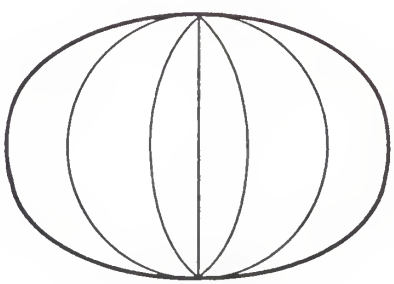

$\beta_2<0$

FIGURE 1

EXPLANATION OF FIGURE 2

Magnitude and sign of the quadrupole deformation for the nucleus in the region of A = 28.

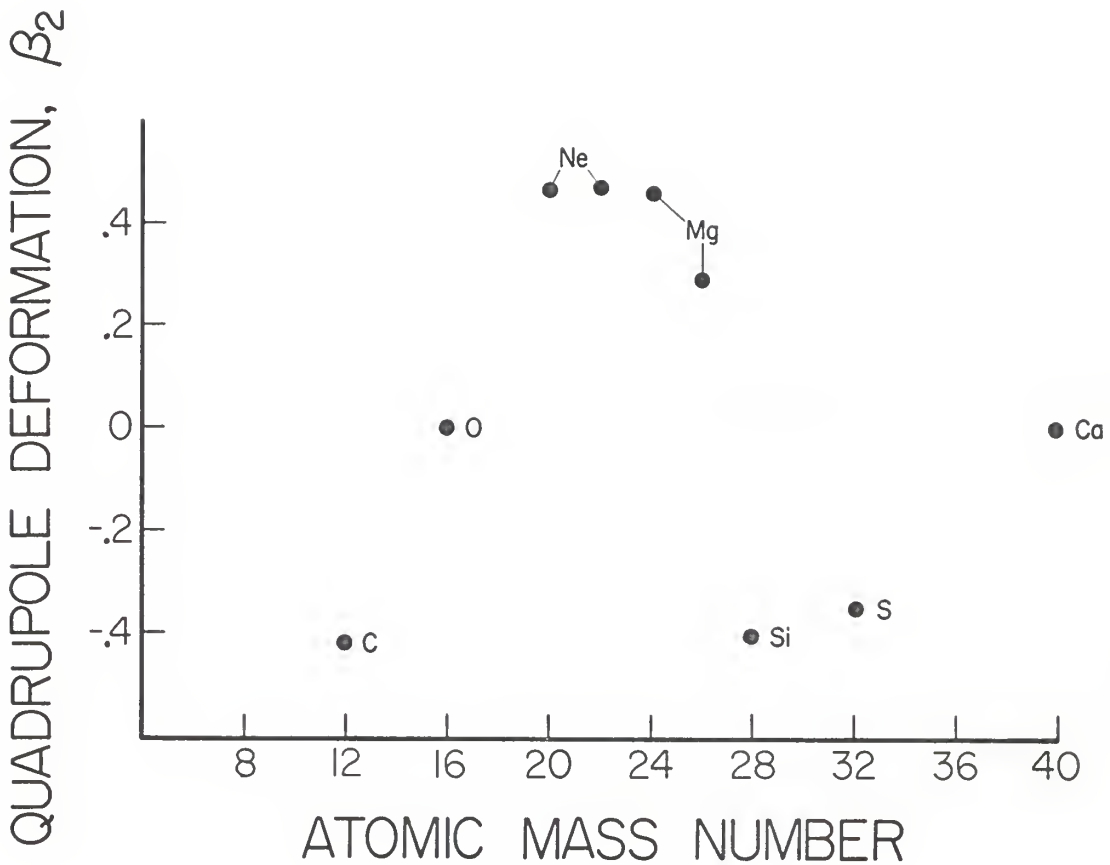
QUADRUPOLE DEFORMATION, β_2
.4
.2
0
-.2
-.4
Ne
Mg
O
Ca
C
Si
S
8
12
16
20
24
28
32
36
40
ATOMIC MASS NUMBER

FIGURE 2

the nucleus will have rotational excitation levels at a finite energy and these levels may be excited in an inelastic scattering process. One can picture this process classically as occuring through the exertion of a torque on the deformed target nucleus by the passing projectile which then causes the target nucleus to rotate. The force which gives rise to the torque may be either the Coulomb force (Coulomb excitation), the nuclear force or both. Since the total angular momentum must be conserved during the scattering process the relative orbital angular momentum of the target and projectile decreases while the spin angular momentum of the deformed target increases in such a way that the angular momentum conservation law is satisfied. The excitation process and related scattering cross sections depend strongly on the deformation of the target nucleus and therefore, can be used to determine the deformation (the shape) of the target nucleus.

In the shell theory, the nucleons of the nuclei in the region of A=28 occupy the 2s-1d shell. The elastic and inelastic cross sections of the scattering process of a wide range of projectile nuclei, A_p between 1 and 40, from a 2s-1d target nucleus were used to determine the shape of the target nucleus. It has been found that each different projectile nucleus yields a different measured deformation due to the fact that it is the potential deformation which is determined by the numerical analyses. The radius of the potential surface can be described by:[2]

$$R = R_o(\Delta) + \delta_2(\Delta)Y_{20}(\theta) \qquad (2)$$

where:

$$R_0(\Delta) = r_0(A_t^{1/3} + A_p^{1/3})$$

Δ = equivalent uniform charge radius of projectile

$\delta_2(\Delta)$ = quadrupole deformation length.

It should be noted that to the lowest order in Δ/R_o, the quadrupole deformation length, $\delta_2(\Delta)$, is independent of Δ. Also, the nuclear potential deformation, β_2^n, can be obtained using:

$$\delta_2(0) = \beta_2^n r_o A_t^{1/3} \tag{3}$$

and the geometrical arguments as presented in papers by Hendrie[3] and later by Thompson and Eck.[4] It has been shown that the measured deformation parameters for the cases of ^{20}Ne, ^{24}Mg and ^{28}Si with different bombarding projectile nuclei are consistent with each other, if the appropriate geometric corrections are applied. However, in the case of $^{16}O+^{28}Si$ scattering, the measured deformation length is consistently lower[4] than what is predicted by the systematics. Because of this apparent deviation from systematics, it was decided to investigate in greater detail the case of $^{16}O+^{28}Si$ scattering.

In this work, both elastic and inelastic scattering cross sections were obtained for the ^{16}O bombarding energies of 32, 34, 36 and 40 MeV for laboratory angles 15 to 75 degrees. These scattering cross sections were normalized to the excitation functions that were measured at laboratory angles of 30, 45 and 70 degrees for ^{16}O bombarding energies of 24 to 40 MeV (see Section III A).

The measured elastic scattering cross sections were analyzed using an optical model in order to obtain the best description of the measured cross sections. The optical model parameters obtained are then compared to the optical model parameters for $^{16}O+^{28}Si$ scattering obtained from other research workers.

The inelastic scattering cross sections show strong Coulomb-nuclear interference effects (explained in more detail in Section IV) and could

be used in more sophisticated analyses involving coupled channels calculations to determine the nuclear shape of ^{28}Si. These cross sections are presented in Section III.

II. EXPERIMENTAL PROCEDURE

A. ^{16}O Beam

The ^{16}O beam used in this work was obtained by first introducing distilled water vapor into a High Voltage Engineering Corporation Diode Ion Source operating at about 50 kV with a 110 Amp hydrogen arc. This produced the ^{16}O ions, which were accelerated by the Kansas State 6MV model EN Tandem Van de Graaff Accelerator to the desired bombarding energies of 32, 34, 36 and 40 MeV. A 90 degree analyzing magnet selected the desired energy and charge state for the ^{16}O ion beam. A switching magnet steered the ^{16}O ion beam into the target chamber.

B. Target Chamber

A stainless steel target chamber[5] of 24" (61.0 cm) diameter and capable of obtaining a vacuum in the μtorr range was used for this scattering experiment. The chamber has such features as a rotatable target holder, a target air lock, plus external controls for target and detector orientation. The target holder can hold up to five targets, which can be isolated from the rest of the chamber by an air lock. Up to eight detectors can be placed on three concentric rings, which can be externally turned to the desired angle between the incoming and scattered beams. Just before the entrance to the chamber, there were two tantalum collimators held in a 18" (45.7 cm) long stainless steel sleeve placed in the beam line. Both of the collimators had a $\frac{11}{32}$" (8.7 mm) diameter hole in order to collimate the beam. Before each detector, there were two tantulum collimators and each had a $\frac{1}{16}$" x $\frac{3}{8}$" (1.6 x 9.5 mm) slit. This gave an angular resolution of less than one degree at any detector.

EXPLANATION OF FIGURE 3

Side view section drawing of target chamber.

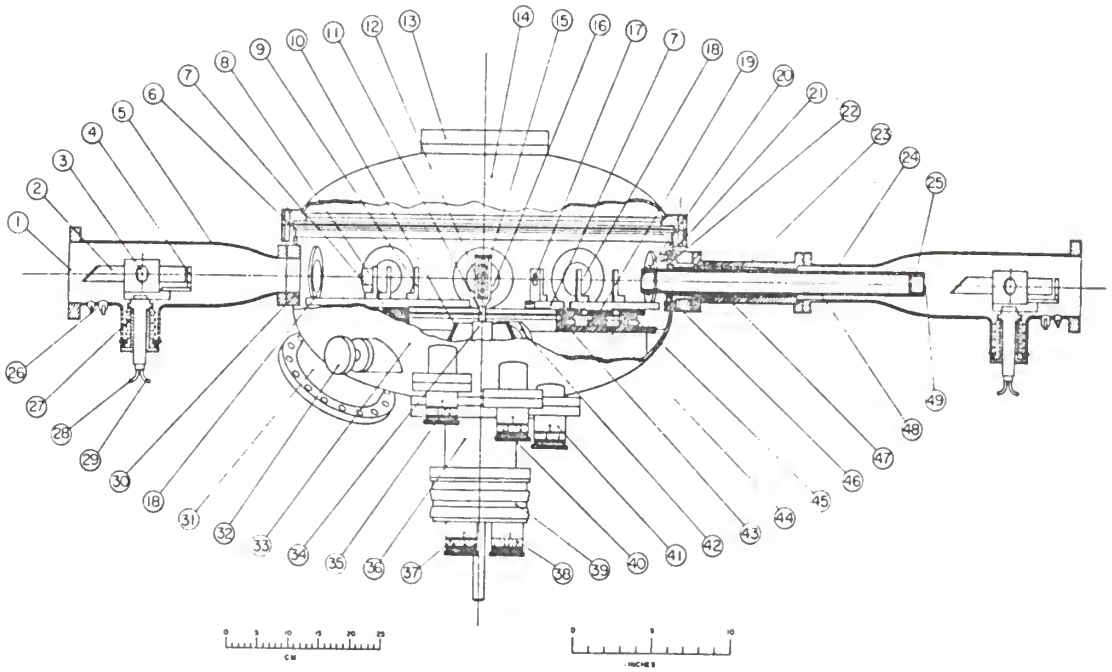

1. 4" diam. port for down-beam experiments
2. Faraday cup
3. Vicor viewing disk
4. Electron supressor ring
5. Faraday cup-beam viewer housing
6. Aluminum gasket
7. Detector mounting track
8. Particle detector
9. Detector mount
10. Target air lock valve housing
11. Target rod
12. Target ladder
13. 6" diam. port blank-off
14. Chamber lid
15. Target
16. 2" diam. port
17. Detector collimator
18. 2" diam. port
19. Radial ball bearing
20. Anti-scattering slit
21. Thumb screw for collet release
22. Collet hinge
23. Collet housing
24. Faraday cup-beam viewer housing
25. Electrically insulated insert
26. Electrical feedthroughs
27. Bellows
28. Water inlet
29. Water return
30. 2" diam. beam exit port
31. 6" diam. pumping port
32. Air-lock valve control
33. Chamber housing
34. Target housing
35. Detector positioning control
36. Target air-lock extension
37. Target orientation control
38. Target selection control
39. Electrical insulator
40. Detector positioning control
41. Detector positioning control
42. Swing-valve cover
43. Mounting platform
44. Ball bearing retainer
45. Rotatable mounting ring
46. Beam collimator insert
47. Tapered collet
48. Beam collimator tube
49. Beam collimator insert

FIGURE 3

C. Targets

The targets used were self-supporting SiO_2 targets prepared at Kansas State University from a SiO_2 powder in which ^{28}Si was enriched to 99.899% of all the silicon present in the powder by the Oak Ridge National Laboratory. The target thickness varied from 50 to 100 $\mu g/cm^2$.

The targets were prepared by first evaporating the SiO_2 powder off a tungsten ribbon, which was located in a vacuum chamber, onto a glass slide coated with a liquid soap, Teepol. A small amount of tungsten was evaporated along with the SiO_2. This produced an ^{16}O + W elastic scattering peak in the measured scattering spectra (see Figure 4). The yield from this peak enabled us to normalize the ^{16}O + ^{28}Si scattering cross sections (see Section III A). After removal from the vacuum chamber, the glass slides were etched so that the SiO_2 film was cut into small rectangles. The SiO_2 film rectangles were floated off the glass slide by twos, and each was mounted on a target frame which had a $\frac{11"}{32}$ (8.7 mm) diameter hole in its center. The completed targets were allowed to dry before being placed in the target chamber.

D. Detectors and Other Electronics

Ortec surface barrier detectors with 100 μm sensitive depth were used to detect the scattered ^{16}O particles. As schematically shown in Figure 5, we used an Ortec 109A Preamplifier and an Ortec 451 Spectroscopy Amplifier to amplify the pulses from the surface barrier detector. The bias voltage source for the detector was an Ortec 210 Detector Control Unit. The amplified pulses were analyzed by a Canberra 8100 Multichannel Analyzer (M.C.A.) into a 1024 channel spectrum. A typical pulse height spectrum is shown in Figure 4. The M.C.A. can accumulate simultaneously up to eight separate spectra. These spectra were transferred to the memory

FIGURE 4

A typical pulse-height spectrum for ^{16}O scattering from the $^{28}SiO_2$ targets described in the text. The elastic and inelastic (2^+, Q = -1.78 MeV) scattering peaks for ^{16}O + ^{28}Si are well resolved. The ^{16}O + W elastic peak was used for normalization purposes.

FIGURE 4

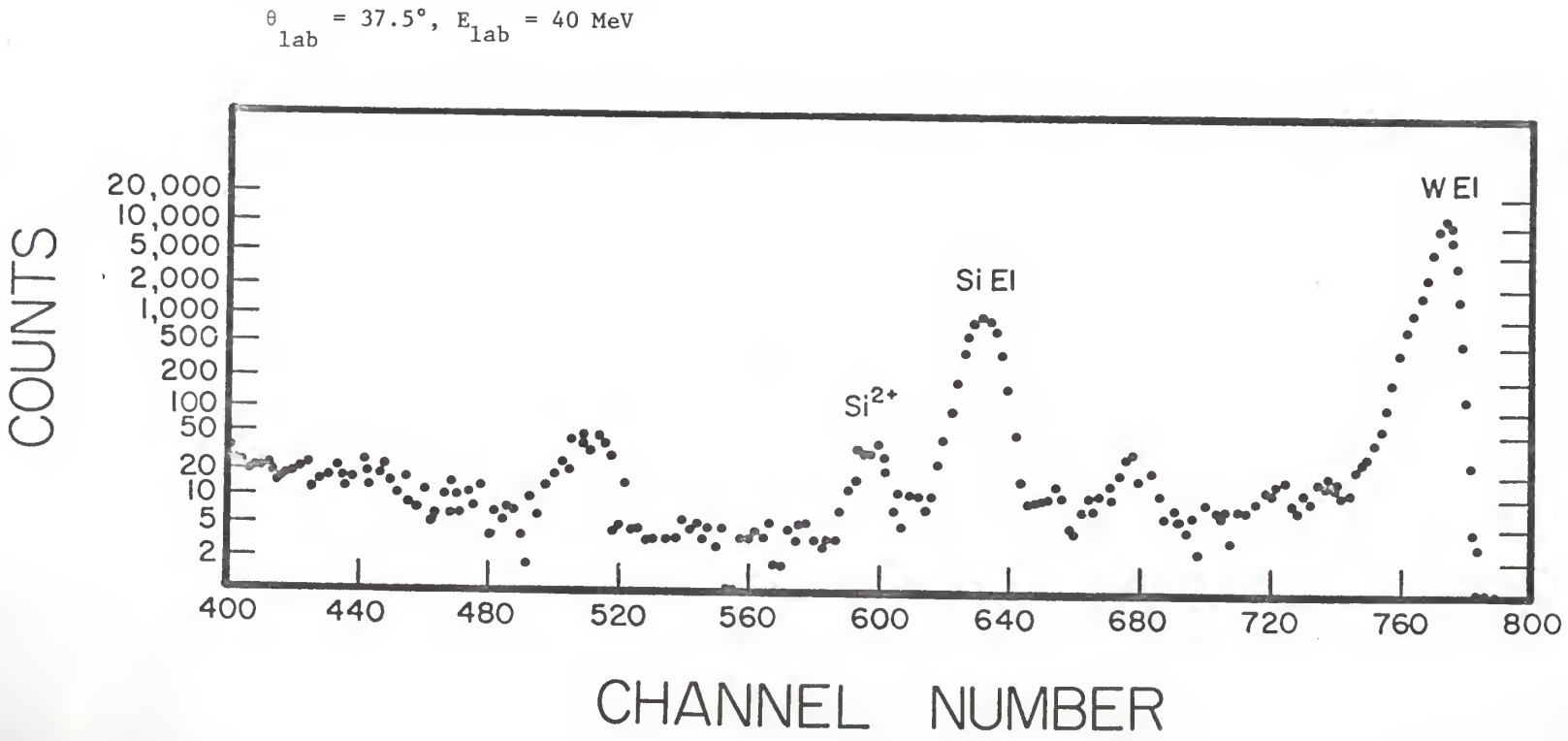
θ_{lab} = 37.5°, E_{lab} = 40 MeV
COUNTS
20,000
10,000
5,000
2,000
1,000
500
200
100
50
20
10
5
2
Si EI
Si^{2+}
W EI
400
440
480
520
560
600
640
680
720
760
800
CHANNEL NUMBER

EXPLANATION OF FIGURE 5

Schematic of electronics.

FIGURE 5

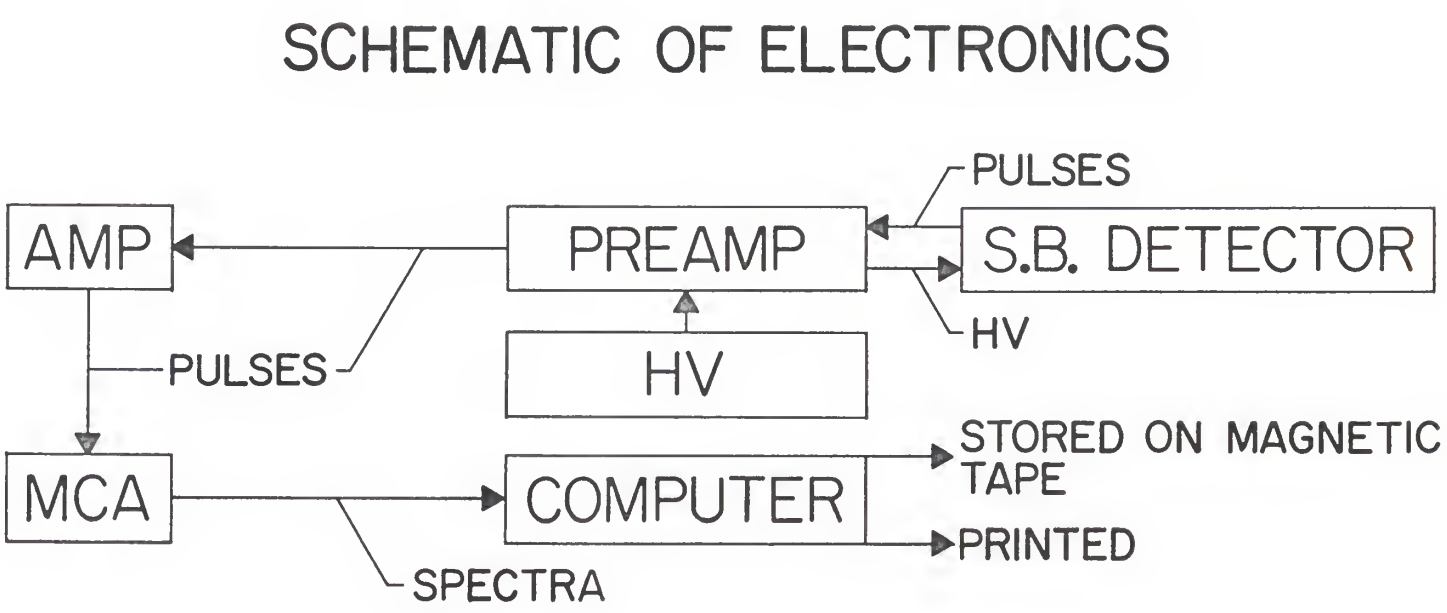
SCHEMATIC OF ELECTRONICS
PULSES
AMP
PREAMP
S.B. DETECTOR
HV
PULSES
HV
STORED ON MAGNETIC TAPE
MCA
COMPUTER
PRINTED
SPECTRA

of a PDP-15 computer so that they could be stored on magnetic tape for further analysis and display purposes. All spectra were printed out to obtain a hard copy.

III. ANALYSIS

A. Determination of Elastic Scattering Cross Sections

Using two body kinematics we identified the $^{16}O + W$ and $^{16}O + ^{28}Si$ elastic scattering peaks as well as the $^{16}O + ^{28}Si$ inelastic ($2^+, Q = -1.78$ MeV) scattering peak. The yields for all these peaks were extracted by a PDP-15 computer program[6] that can fit up to four separate skewed Gaussian curves simultaneously with a linear background from the pulse height spectra. This program also gave the error in its evaluation of each yield. The errors extracted were carried on through all calculations to give the errors for the scattering cross sections. A typical spectrum and the fitted Gaussian curves are shown in Figure 6.

It is simpler to describe theoretically a scattering process in the center of mass coordinate system than it is to describe it in the laboratory coordinate system. One can find the center of mass scattering angle from one of the following relations between the scattering angle in the center of mass system θ_{cm} and in the laboratory system θ_{lab}:[7]

$$\theta_{cm} = \arcsin\left[\frac{m_p}{m_t}\sin(\theta_{lab})\right] + \theta_{lab} \tag{4}$$

$$\tan(\theta_{lab}) = \frac{m_t \sin(\theta_{cm})}{m_p + m_t \cos(\theta_{cm})} \tag{5}$$

Where: m_p = mass of projectile

m_t = mass of target

In an elastic scattering process, the equation that determines the number of particles that are scattered at a particular angle is:[8]

EXPLANATION OF FIGURE 6

The Gaussian curves for the $^{16}O + ^{28}Si$ elastic and inelastic (Q = -1.78 MeV) scattering peaks and the ^{16}O + W elastic scattering peak found in the typical pulse height spectrum.

FIGURE 6

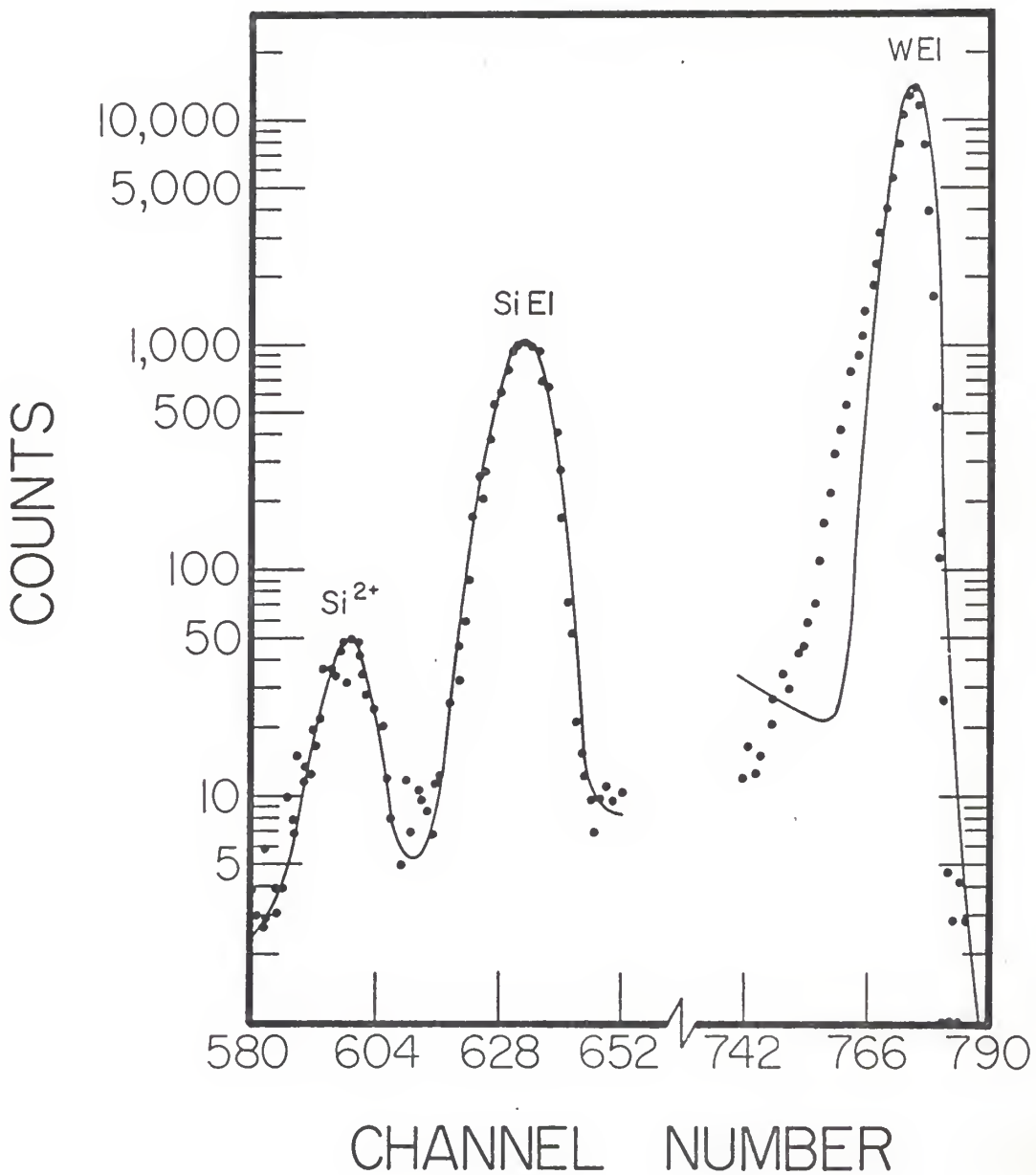
COUNTS
10,000
5,000
1,000
500
100
50
10
5
Si 2+
Si EI
WEI
580
604
628
652
742
766
790
CHANNEL NUMBER

$$Y_{el}(\theta_{lab}) = a\sigma_{el}(\theta_{cm})\, nN_i \left(\frac{d\Omega_{lab}}{d\Omega_{cm}}\right)_{el} \qquad (6)$$

Where:

Y_{el} = number or yield of detected scattered particles

a = constant dependent on detector efficiency and the geometry of the target chamber set up

σ_{el} = elastic scattering cross section

n = thickness (units of target nuclei/cm^2)

N_i = number of incident particles on foil

$\left(\frac{d\Omega_{lab}}{d\Omega_{cm}}\right)_{el}$ = elastic scattering solid angle correction

A solid angle correction was applied because the detector subtents a different solid angle in the center of mass system than it does in the laboratory system. With the help of Equations (4) and (5), it can be shown that:

$$\left(\frac{d\Omega_{lab}}{d\Omega_{cm}}\right)_{el} = \frac{\sin(\theta_{lab})d\theta_{lab}}{\sin(\theta_{cm})d\theta_{cm}} = \frac{\sin^2(\theta_{lab})\cos(\theta_{cm} - \theta_{lab})}{\sin^2(\theta_{cm})} \qquad (7)$$

Applying Equation (6) to $^{16}O + {}^{28}Si$ and $^{16}O + W$ elastic scattering the following ratio is obtained:

$$\frac{\sigma_{el}^{si}}{\sigma_{el}^{w}} \cdot \frac{n_{si}}{n_w} = \frac{Y_{el}^{si}}{Y_{el}^{w}} \frac{\left(\frac{d\Omega_{cm}}{d\Omega_{lab}}\right)_{el}^{si}}{\left(\frac{d\Omega_{cm}}{d\Omega_{lab}}\right)_{el}^{w}} \equiv R(\theta_{lab}) \qquad (8)$$

In this work, all bombarding energies were well below the Coulomb barrier for $^{16}O + W$ scattering. As a result, it can be written that:

$$\sigma_{el}^{w} = \sigma_r^{w} = k'/\sin^4\left(\tfrac{1}{2}\ \theta_{cm}^{w}\right) \qquad (9)$$

Where:

k' = constant

σ_r = Rutherford cross section

Multiplying Equation (8) by Equation (9) and then dividing the product by:

$$\sigma_r^{si} = k''/\sin^4(\tfrac{1}{2}\,\theta_{cm}^{si}) \tag{10}$$

one obtains:

$$\frac{\sigma_{el}^{si}}{\sigma_r^{si}} = \frac{k'}{k''}\,\frac{n_w}{n_{si}}\,\frac{\sin^4(\frac{1}{2}\,\theta_{cm}^{si})}{\sin^4(\frac{1}{2}\,\theta_{cm}^{w})}\,R(\theta_{lab}) \tag{11}$$

This equation can be rewritten in the following form:

$$\frac{\sigma_{el}}{\sigma_r} = KR'(\theta_{lab}) \tag{12}$$

Note that the "si" superscript in Equation (12) was dropped for convenience. At bombarding energies less than the Coulomb barrier, the ^{16}O + ^{28}Si elastic cross section σ_{el} should be equal to the ^{16}O + ^{28}Si Rutherford cross section σ_r. So, K must be chosen so that:

$$\frac{\sigma_{el}}{\sigma_r} = KR'(\theta_{lab}) = 1 \tag{13}$$

for energies and angles where it may be assumed that the ^{16}O + ^{28}Si scattering is pure Rutherford.

Given the above discussion, $R'(\theta_{lab})$ was determined for θ_{lab} = 30, 45 and 75 degrees with the bombarding energy range between 24 and 40 MeV. K was then chosen so that the mean of $KR'(30°)$ for bombarding energies of 24, 26 and 28 MeV is equal to one. Calling this K, K_θ the following

EXPLANATION OF FIGURE 7

Excitation Function of $(\sigma_{el}/\sigma_r)_\theta$ for $^{16}O + ^{28}Si$ at the laboratory angles at 30°, 45°, and 70° in the bombarding energy range from 24 to 40 MeV. Also shown are the optical model curves as solid lines.

FIGURE 7

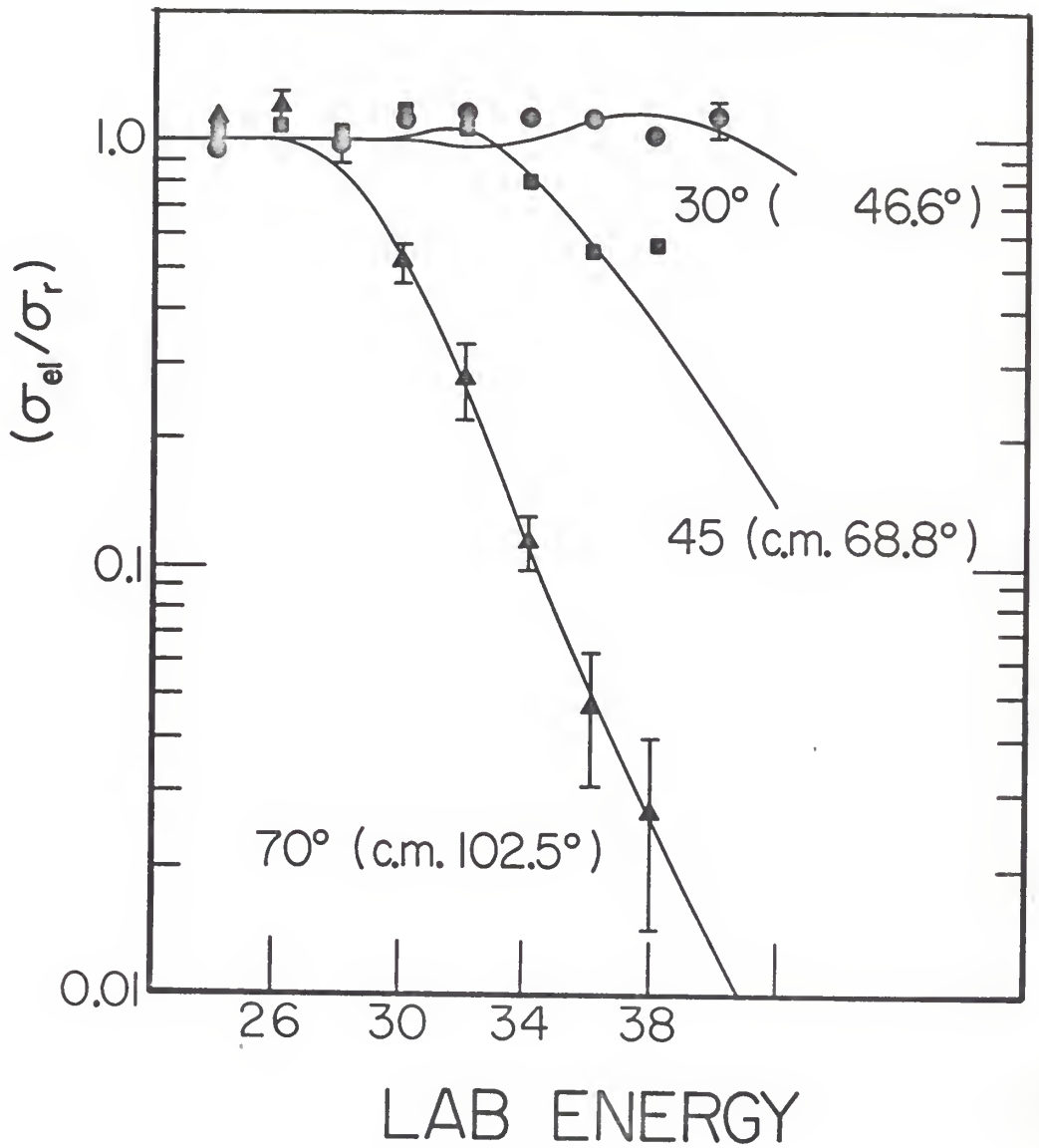
1.0
0.1
0.01
(σ_{el}/σ_r)
30° (46.6°)
45 (c.m. 68.8°)
70° (c.m. 102.5°)
26
30
34
38
LAB ENERGY

equation can be used

$$\left(\frac{\sigma_{el}}{\sigma_r}\right)_\theta = K_\theta R_\theta'(\theta_{lab}) \qquad (14)$$

We are using the subscript "θ" to signify that θ_{lab} was held constant while the energy was varied. The normalized values of $(\sigma_{el}/\sigma_r)_\theta$ as a function of ^{16}O bombarding energies are defined to be the Excitation Function of $(\sigma_{el}/\sigma_r)_\theta$ for a particular scattering angle. Figure 7 shows the Excitation Function for 30°, 45° and 70° in the bombarding energy range from 24 to 40 MeV.

Later values of $KR'(\theta_{lab})$ will be called $K_E R_E'(\theta_{lab})$ since the ^{16}O bombarding energies were held constant while θ_{lab} was varied. $K_E R_E'(\theta_{lab})$ values were determined for ^{16}O bombarding energies at 32, 34, 36 and 40 MeV for θ_{lab} between 15 and 75 degrees. K_E for a particular bombarding energy was chosen so that the values of $K_E R_E'(\theta_{lab})$ were normalized to the Excitation Functions of $(\sigma_{el}/\sigma_r)_\theta$. The following equation can be used to find $(\sigma_{el}/\sigma_r)_E$ from the normalized values of $K_E R_E'(\theta_{lab})$:

$$\left(\frac{\sigma_{el}}{\sigma_r}\right)_E = K_E R_E'(\theta_{lab}) \qquad (15)$$

The normalized $(\sigma_{el}/\sigma_r)_E$ points as a function of θ_{cm}^{si} are defined to be the Angular Distribution of $(\sigma_{el}/\sigma_r)_E$ for a particular ^{16}O bombarding energy. Figure 8 shows the angular distributions for the ^{16}O bombarding energies of 32, 34, 36 and 40 MeV.

B. The Optical Model Theory

All bombarding energies used in this work were in the neighborhood of the Coulomb barrier for $^{16}O + ^{28}Si$, which is about 28 MeV. If the

EXPLANATION OF FIGURE 8

Angular distribution of $(\sigma_{el}/\sigma_r)_E$ for $^{16}O + ^{28}Si$ at the ^{16}O bombarding energies at 32, 34, 36 and 40 MeV. Also shown are the optical model curves as solid lines.

FIGURE 8

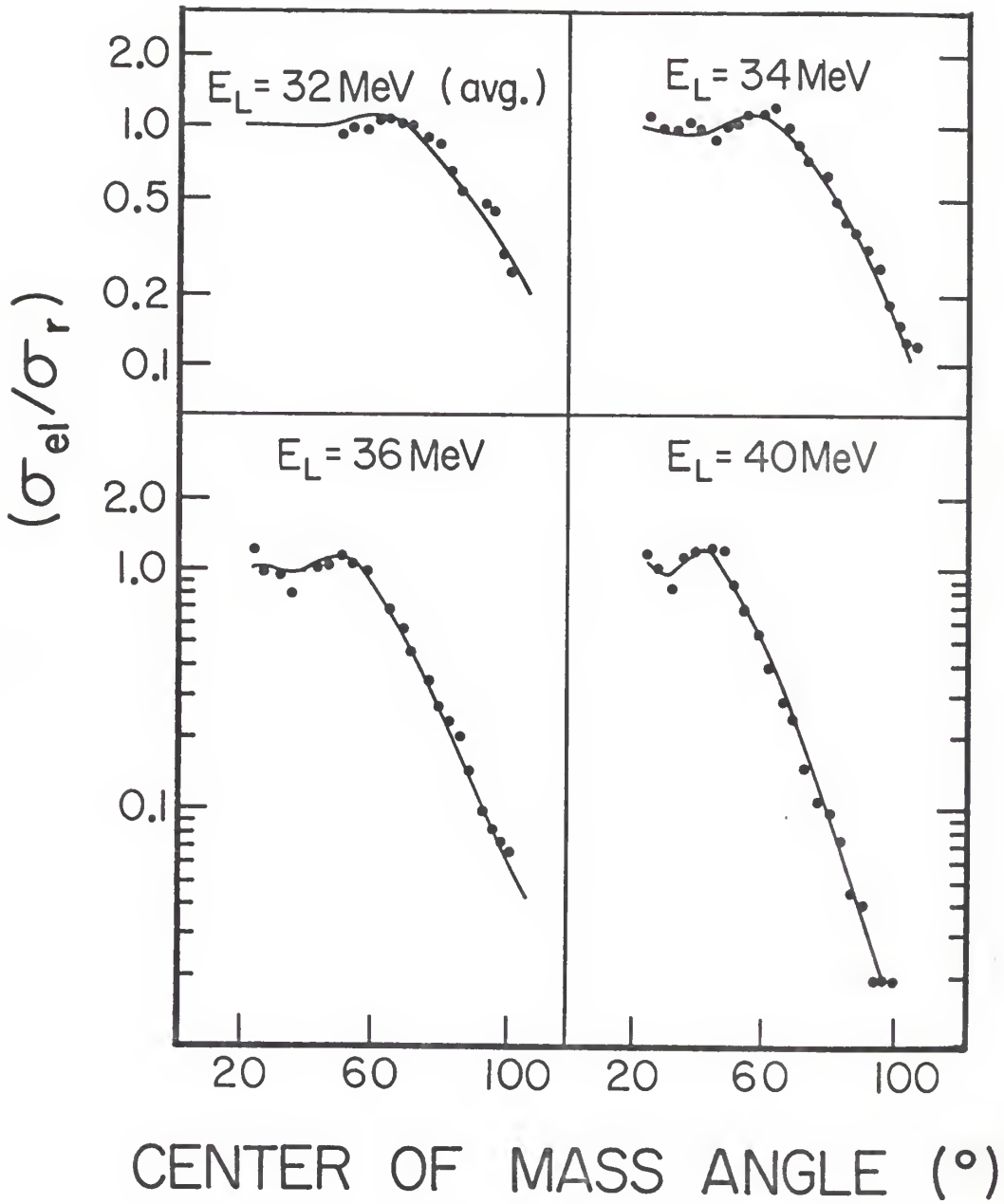
E_L = 32 MeV (avg.)
E_L = 34 MeV
E_L = 36 MeV
E_L = 40 MeV
2.0
1.0
0.5
0.2
0.1
(σ_{el}/σ_r)
20
60
100
CENTER OF MASS ANGLE (°)

target nucleus is assumed to be spherical*, the elastic cross sections can be fitted by an optical model potential that has the following form:[9]

$$V = V_c(r) - \frac{V_o}{1+\exp((r-R_o)/a_o} - \frac{iW_o}{1+\exp((r-R_w)/a_w)} \qquad (16)$$

where:

$$R_o = r_o(A_p^{1/3} + A_t^{1/3})$$

$$R_w = r_w(A_p^{1/3} + A_t^{1/3})$$

$$V_c(r) = \begin{cases} Z_p Z_t e^2[3-(r/R_o)^2]/2R_o & r \leq R_o \\ Z_p Z_t e^2/r & r \geq R_o \end{cases}$$

V_o, W_o = real and imaginary potential strengths

a_o, a_w = real and imaginary diffuseness parameters

r_o, r_w = real and imaginary radius parameters

$V_c(r)$ = Coulomb potential

p,t = subscripts meaning projectile and target.

The parameters V_o, W_o and a_w were varied to obtain the best chi squared fit to the angular distributions of the $^{16}O + ^{28}Si$ elastic scattering cross sections. The other parameters were not varied and were determined from previous analysis of $^{16}O + ^{28}Si$ elastic scattering studies.[2,9] An optical model program developed by Choi and Thompson[10] was used to extract the varied parameters. The resultant optical model curves and the angular distributions of $(\sigma_{el}/\sigma_r)_E$ are shown in Figure 8 while in Figure 7 are shown the optical curves and the excitation functions of $(\sigma_{el}/\sigma_r)_\theta$.

C. Determination of Inelastic Scattering Cross Sections

The inelastic (Q=-1.78 MeV) scattering cross sections, σ_{2+} for a

EXPLANATION OF FIGURE 9

The inelastic cross section, σ_{2+}, as a function of the 2^+ inelastic center of mass angle for silicon.

FIGURE 9

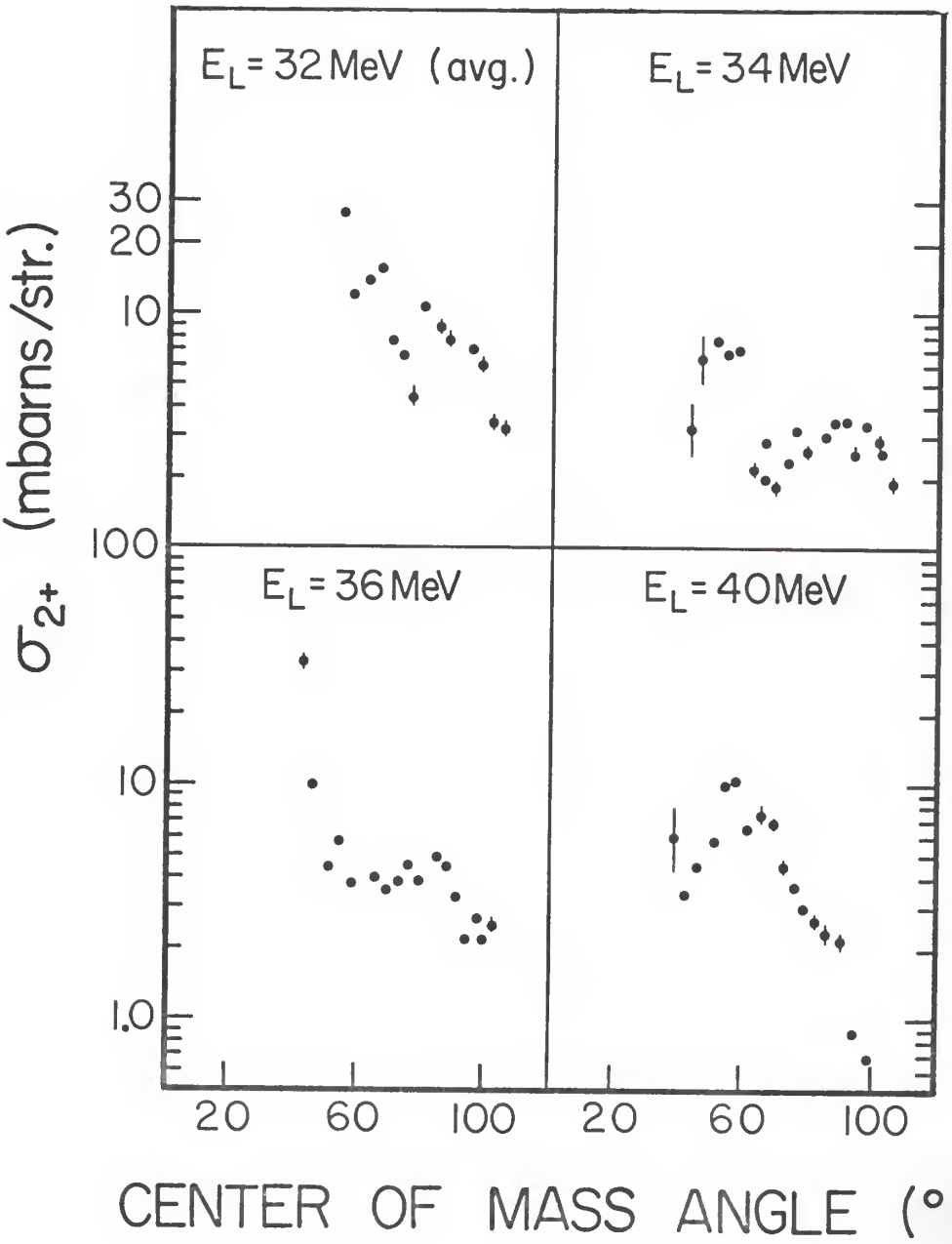
E_L = 32 MeV (avg.)
E_L = 34 MeV
E_L = 36 MeV
E_L = 40 MeV
σ2+ (mbarns/str.)
30
20
10
100
10
1.0
20
60
100
20
60
100
CENTER OF MASS ANGLE (°)

particular energy and angle were determined from the following equation:

$$\sigma_{2+} = \frac{Y^{si}_{2+}}{Y^{si}_{el}} \cdot \frac{(d\Omega_{cm}/d\Omega_{lab})^{si}_{2+}}{(d\Omega_{cm}/d\Omega_{lab})^{si}_{el}} \left(\frac{\sigma_{el}}{\sigma_r}\right)_E \cdot \sigma_r \qquad (17)$$

Where:

Y^{si}_{2+} = inelastic (2^+) scattering yield for $^{16}O + ^{28}Si$

$\left(\frac{d\Omega_{cm}}{d\Omega_{lab}}\right)^{si}_{2+}$ = ^{28}Si inelastic (2^+) solid angle correction

Since $(\sigma_{el}/\sigma_r)_E$ has already been normalized, σ_{2+} is also normalized when Equation (17) is used. The resultant values of σ_{2+} versus θ^{2+}_{cm} for various ^{16}O bombarding energies are shown in Figure 9.

IV. DISCUSSION OF RESULTS

Looking at the inelastic scattering cross sections in Figure 9 for 34 and 36 MeV one will note that a common characteristic is a peak at forward angles followed by a minimum and then a secondary maximum. Comparing the inelastic scattering cross sections to their respective elastic scattering cross sections, found in Figure 8, shows that the mimimum occurs roughly where $(\sigma_{el}/\sigma_r)_\theta$ has a maximum. The $(\sigma_{el}/\sigma_r)_\theta$ maximum occurs right before the $(\sigma_{el}/\sigma_r)_\theta$ curve begins to fall off exponentially. It is also noted that this same behavior occurs for the 32 and 40 MeV cross sections but it is not as pronounced as for 34 and 36 MeV. This same behavior was noted by Gale[11] and Videbaek et. al.[12]

This behavior[12,13] can be explained by a semiclassical description of the scattering process in terms of Coulomb and nuclear effects plus interference between the Coulomb and nuclear forces. The inelastic scattering (or excitation) amplitude, f, has the form:

$$f = i(f_C + f_R) + f_I \tag{18}$$

Where:

f_C = Coulomb excitation amplitude

f_R, f_I = real and imaginary (absorption) nuclear excitation amplitudes

The inelastic scattering cross sections, σ_{2+}, can be determined using these amplitude since:

$$\sigma_{2+} \propto |f|^2 = |f_C + f_R|^2 + |f_I|^2 \tag{19}$$

$$\sigma_{2+} \propto |f_C|^2 + |f_R|^2 + |f_I|^2 + 2f_C f_R \tag{20}$$

Since the Coulomb force is repulsive in the scattering of two nuclei, and the nuclear force is attractive, f_C and f_R have opposite signs. At forward angles, or low energies, the $|f_C|^2$ term dominates Equation (20). As the angle, or energy, is increased, both $|f_C|$ and $|f_R|$ change, but $|f_R|$ changes more rapidly (increases) which result in the observed minimum in the inelastic cross section curve.

There is also an interference in the elastic scattering cross sections which can be explained by a similar analysis; but due to differences in the scattering amplitudes, we have a constructive interference instead of a destructive interference for the same angular region. The fact that the elastic and the 2+ inelastic interference patterns are 180 degrees out of phase has been discussed by Blair.[13] By measuring the interference between nuclear and Coulomb scattering it is possible to determine the nuclear scattering amplitude in the presence of the more dominant Coulomb scattering. Furthermore, the interference effects are a sensitive measure of the nuclear and Coulomb deformation parameters as shown by Videbaek[12] and many others.

Listed in Table 1 are the Optical Model potential parameters obtained from our analysis of the elastic scattering cross sections of $^{16}O + ^{28}Si$. Also listed, are the results obtained from other workers.

Table 1. Optical Model Parameters for the Elastic Scattering $^{16}O + {}^{28}Si$.

E_{lab} (MeV)	V_o (MeV)	W_o (MeV)	r_o† (fm)	r_w (fm)	a_o (fm)	a_w (fm)	Reference
32,34 36,40	23.44	4.91	1.31	1.31	0.49	0.652	Pres. Work
33,36 & 38	16.75	7.00	1.35	1.35	0.49	0.38	9
33	18.00	4.00	1.31	1.31	0.49	0.38	2
36	22.00	4.00	1.31	1.31	0.49	0.38	2
38	23.00	4.00	1.31	1.31	0.49	0.38	2
40	14.00	5.00	1.35	1.35	0.49	0.38	14
55	21.50	6.25	1.35	1.35	0.49	0.38	14
33 thru 215.2	10.00	23.4	1.35	1.23	0.618	0.552	15

†Note that the O.M. fitting program that was used was originally written for proton scattering so that in the program $R_o = r_o' A_t^{1/3}$. The r_o listed here gives the same R_o using the equation for R_o under Equation (16), thus: $r_o = r_o' A_t^{1/3}/(A_t^{1/3} + A_p^{1/3})$. Likewise for r_w.

V. CONCLUSIONS

The elastic and inelastic (2^+, Q = 1.78 MeV) scattering cross sections were determined for the scattering of ^{16}O from ^{28}Si. The scattering cross sections show strong Coulomb-nuclear interference. This is seen in the elastic cross section by the deviation of the elastic cross sections from pure Rutherford scattering and in the inelastic cross sections at intermediate angles as a rapid fluctuation from pure Coulomb excitation.

The parameters for the optical model potential were also determined, and were found to be approximately equal to the parameters determined by others.

The angular distributions of the inelastic cross sections scattered to the lowest 2^+ state of ^{28}Si measured here can be used by later workers in a combined coupled channels-optical model analysis in order to determine the values of the quadrupole deformation, β_2, and the deformation length, δ_2, for $^{16}O + ^{28}Si$. Because of the strong Coulomb-nuclear interference effects, the cross sections should prove to be a sensitive measure of the nuclear deformation parameters. It should be possible to check the consistency of these deformation parameters with the systematic values determined earlier.

The main difficulty in carrying out this work was the extraction of the yields for the inelastic peaks due to the low count rates and the small signal to noise ratio.

REFERENCES

*Note that the ^{28}Si nucleus is not spherical but is an oblate spheroid. The parameters obtained using the above potential can be used for the first approximation.

1. Y. Abgrall, B. Morand and E. Caurier, Nucl. Phys. A192, 372 (1972). M. P. Fricke and G. R. Satchler, Phys. Rev. 139, B567 (1965). H. R. E. Tjin, A. Djie, K. Mulder, F. Udo, A. Groenveld, L. A. Ch. Koertz, A. D. Hill and P. E. Hodgson, Nucl. Phys. A106, 85 (1968).
2. J. S. Eck, D. O. Elliott, W. J. Thompson and F. T. Baker, Phys. Rev. C 16, 1020 (1977).
3. D. L. Hendrie, Phys. Rev. Letters 31, 478 (1973).
4. W. J. Thompson and J. S. Eck, Phys. Letters 67B, 151 (1977).
5. For another description of this chamber see: E. J. Feldl, Nucl. Inst. and Meth. 117, 5 (1974).
6. Computer program "XRAYMT" by J. C. Legg, Kansas State University.
7. R. D. Evans, The Atomic Nucleus (McGraw-Hill, New York, 1955) p. 834.
8. P. T. Weider and R. L. Sells, Elementary Modern Physics, 2nd Ed. (Allyn and Bacon, Boston, 1968) p. 226.
9. D. S. Gale and J. S. Eck, Phys. Rev. C 7, 1950 (1973).
10. Triangle Universities Nuclear Laboratory's version two of computer program "SNOOPT2", written by B. H. Choi and W. J. Thompson, Dept. of Physics, University of North Carolina at Chapel Hill; Private Communication.
11. D. S. Gale, Kansas State University Doctorate Thesis (1972). Data from this thesis can be found in Ref. 9.

12. F. Videbaek, I. Chernov, P. R. Christensen and E. E. Gross, Phys. Rev. Letters 28, 1072 (1972).

13. J. S. Blair, Direct Interactions and Nuclear Reaction Mechanism, edited by E. Clementel and C. Villi (Gordon and Breach, New York 1963) p. 669.

14. R. H. Siemssen, Argonne National Laboratory Report No. ANL-7837, 1971 p. 145.

15. J. G. Cramer, R. M. DeVries, D. A. Goldberg, M. S. Zisman and C. F. Maguire, Phys. Rev. C 14, 2158 (1970).

ACKNOWLEDGEMENTS

The author wishes to acknowledge the many people who have made this work possible. Particularly:

Dr. John S. Eck, for his advice, assistance, and encouragement;

Dr. James C. Legg for help with computer programming;

James N. Wickberg, Robert L. Philips and Glen S. Gealy for their help;

My wife, Pamela.

STUDY OF ELASTIC AND INELASTIC SCATTERING OF ^{16}O BY ^{28}Si

by

ROBERT R. BRUCKMAN

B. A., Hastings College, 1976

An Abstract of

A MASTER'S THESIS

submitted in partial fulfillment of the

requirements for the degree

MASTER OF SCIENCE

Department of Physics

Kansas State University

Manhattan, Kansas 66506

1978

ABSTRACT

The elastic and inelastic (2+, Q = -1.78 MeV) scattering of ^{16}O from ^{28}Si was studied. Angular distributions have been measured for lab energies 32, 34, 36 and 40 MeV. Excitation function measurements were taken at θ_{lab} = 30°, 45° and 70° in the bombarding energy range from 24 to 40 MeV in 2 MeV steps. The optical model parameters that best describe the elastic scattering cross sections were determined and were compared to other parameter sets for the same scattering process. Both elastic and inelastic scattering cross sections showed strong Coulomb-nuclear interference. These cross sections can be used in the extraction of the nuclear deformation parameters utilizing a more sophisticated coupled channels analysis.